Microporous and Mesoporous Materials 265 (2018) 250–257

Contents lists available at ScienceDirect

Microporous and Mesoporous Materials

journal homepage: www.elsevier.com/locate/micromeso

Water vapor adsorption performance of Ag and Ni modified 5A zeolite

W. Henao-Sierra[a], M. Romero-Sáez[b,c], F. Gracia[c], K. Cacua[a], R. Buitrago-Sierra[a,*]

[a] Grupo Materiales Avanzados y Energía, Facultad de Ingeniería, Instituto Tecnológico Metropolitano ITM, Calle 54 A #30-01, Medellín, Colombia
[b] Grupo Calidad, Metrología y Producción, Facultad de Ciencias Económicas y Administrativas, Instituto Tecnológico Metropolitano ITM, Calle 54 A #30-01, Medellín, Colombia
[c] Laboratorio de Catálisis, Facultad de Ciencias Físicas y Matemáticas, Universidad de Chile, Beauchef 851, Santiago, Chile

ARTICLE INFO

Keywords:
Water adsorption
Adsorption enthalpy
Wet impregnation
5A zeolite

ABSTRACT

In this work, Ag and Ni metals incorporation effect on the water adsorption and physicochemical properties of 5A zeolite was studied. For that, Ag/5A and Ni/5A zeolites with different amounts of metal (4, 10 and 20 wt%) were prepared by wet impregnation method. The physicochemical characterization of the adsorbents was carried out by N_2-adsorption, AAS, XRD, FTIR, FE-SEM/EDS, H_2-TPR, CO_2-TPD and TGA-DSC analyses. The results showed that the incorporated metals were well distributed in different sites into the 5A zeolite, without a substantial modification of its crystal structure and morphological characteristics.

Water vapor uptake and water enthalpy adsorption of zeolites were determined simultaneously by a non-isothermal method in a TGA-DSC thermal analyzer, prior saturation of samples with water vapor. It was found that the water molecules adsorption by the metal/zeolites was carried out on different adsorption sites with different interaction energies. Furthermore, it was noted that Ag and Ni metals had a remarkable influence on water adsorption properties of zeolites. Metal addition favored the superficial adsorption of water molecules per available area of zeolite, with high adsorption enthalpy values. This makes the prepared adsorbents potential materials to be used in thermal storage applications and waste heat recovery systems.

1. Introduction

Water adsorption in porous materials is an attractive alternative for waste heat recovery from industrial processes and renewable solar energy uses [1–4]. Porous solid materials such as activated carbon, silica gels, silica-aluminophosphates (SAPOs), metal organics frameworks (MOFs) and zeolites have been widely implemented in refrigeration and thermal storage applications, where water is used as adsorbate [3,4]. For these applications, it is essential to understand the porous material–adsorbate interactions, as well as the required energy for the adsorption-desorption cycles involved in their operation [5].

Zeolites are one of the most widespread sorbents for adsorption processes due to their large surface area, high porosity and reactivity. As well, some zeolites like faujasites (FAU) 10X and 13X and Linde Type A (LTA) zeolites are highly hydrophilic [6]. The sorption behavior of this materials is based on their porous and molecular structure [7], moreover, their water affinity is related to the electrostatic charge of their aluminosilicate framework, due to the Si/Al ratio and the balancing cations [3,4,8].

Additionally, FAU and LTA zeolites are commonly used materials for buildings solar-assisted energy storage. For this application, these zeolites have the disadvantage of high desorption temperatures (> 200 °C) with respect to other materials [4,9]. In last years, several attempts have been made to decrease this temperature and to reduce the strong hydrophilic character of zeolites, by the reduction of the strong interaction between its electrostatically charged framework and the water molecules. These methods involve different strategies as ion exchange [10–12] and variation of Si/Al ratio by dealumination [13,14] or surface silanation [9]. However, this area is under continuous development and the tailoring of the adsorption properties of zeolites by different techniques, is being increasingly studied to satisfy the requirements of different heat transformation cycles [3,4,15].

Metal addition by wet impregnation has been proposed as an alternative to modify the zeolites water adsorption properties. Through this method, metal species are added on the surface, preserving the pristine structure advantages [16]. Metal impregnation has been mainly used to improve the zeolites catalytic properties [17–19], however, to the authors' best knowledge, its effect on the water adsorption properties of zeolites has not been studied yet, in the context of heat recovery and solar heat storage applications.

In this work, 5A zeolite was modified through the incorporation of different amounts of Ag and Ni by wet impregnation. Several

* Corresponding author.
E-mail address: robinsonbuitrago@itm.edu.co (R. Buitrago-Sierra).

https://doi.org/10.1016/j.micromeso.2018.02.036
Received 9 November 2017; Received in revised form 2 February 2018; Accepted 25 February 2018
Available online 02 March 2018
1387-1811/

physicochemical techniques, including AAS, N_2-adsorption, XRD, FTIR, SEM-EDS, H_2-TPR, CO_2-TPD and TGA-DSC analyses, were used to understand the water adsorption behavior of the prepared materials.

2. Experimental

2.1. Materials preparation

5A zeolite (Si/Al:1, CAS No. 69912-79-4, Sigma-Aldrich) was modified through the incorporation of Ag and Ni by wet impregnation method. For this purpose, 2 g of the parent zeolite were added to an aqueous solution of precursor salt ($AgNO_3$ and $Ni(NO_3)_2{\cdot}6H_2O$, Sigma-Aldrich), with the appropriate amount to obtain final samples with 4, 10 and 20 wt% metal. The resulting suspension was heated at 5 °C min^{-1} from room temperature (RT) to 80 °C in an oil bath, and this temperature was kept for 4 h under constant stirring. The solvent was rotoevaporated at 80 °C and the recovered solid was dried at 110 °C for 12 h. Finally, the samples were calcined in air at 550 °C for 6 h, with a heating rate of 20 °C min^{-1}. The obtained materials were designated as XM/5A, where X represents the nominal amount of each metal in wt.%, and M represents the incorporated metal. To confirm the effective amount of Ag and Ni in each zeolite, the solid samples were dissolved in hydrofluoric acid (48 wt%, Sigma-Aldrich). Then, the solutions (0.85–3.78 ppm of metal) were analyzed by Atomic Absorption Spectroscopy (AAS) in a Thermo Scientific iCE 3500 spectrometer.

2.2. Materials characterization

X-ray diffraction (XRD) patterns were recorded in a PANalytical-X'Pert Pro diffractometer, using Cu Kα radiation (λ = 1.54060 Å), from 5° to 60° 2θ degrees, with a step size of 0.1° and a counting time of 5 s per step. For the processing of diffractograms and identification of phases, the PANalytical X'pert HighScore Pro software was used in combination with the International Center for Diffraction Data (ICDD) files.

Diffuse reflectance infrared Fourier transform (DRIFT) spectra were collected in a IRTracer-100 spectrometer, from 2000 to 400 cm^{-1}, with 15 scans and a resolution of 4 cm^{-1}.

Field emission scanning electron microscopy (FE-SEM) and energy dispersive X-Rays spectroscopy (EDS) analyses were carried out in a JEOL JSM-7100F electron microscope, equipped with a silicon drift detector for EDS (X-MAXN, OXFORD). Previous to the analyses, in order to improve the electrical conductivity of samples, they were coated with gold in a sputter coating system (Q300TD, Quorum).

Surface area and porosity of prepared samples were evaluated from the N_2 adsorption-desorption isotherms, determined at −196 °C, in a Micromeritics ASAP 2020 system. Prior to the analysis, the samples (0.10 g) were outgassed at 350 °C for 12 h. Samples total surface area was calculated according to the Brunauer-Emmett-Teller (BET) equation [20], while the t-plot method was used to calculate the volume and surface area of micropores [21]. Total pore volume was calculated from the adsorbed volume at the maximum relative pressure reached by the adsorption isotherm (P/P_o = 0.99).

Temperature-programmed reduction (H_2-TPR) analyses were carried out in a quartz reactor, and the gases were detected by a thermal conductivity detector (TCD). Samples (0.10 g) were first oxidized under a stream of pure O_2 (40 cm^3 min^{-1}) with a temperature ramp of 10 °C min^{-1} from RT to 300 °C. Temperature was maintained at 300 °C for 1 h, and then decreased to RT under the same stream of pure O_2. Finally, the samples were cleaned under a stream of pure Ar (40 cm^3 min^{-1}) at RT. The reducing gas used in all experiments was 5% H_2/Ar, with a flow rate of 20 cm^3 min^{-1}. The temperature range explored was from 50 to 700 °C, with a heating rate of 10 °C min^{-1}. This temperature was maintained for 30 min to complete the reduction process. The water produced by reduction was trapped into a water trap.

Temperature-programmed desorption of CO_2 (CO_2-TPD) experiments were performed on a quartz reactor, and an OmniStar GSD 320 O1 (Pfeiffer Vacuum) mass spectrometer was used to monitor the CO_2 desorption. Prior to adsorption experiments, the samples (0.10 g) were first cleaned under a pure Ar stream (40 cm^3 min^{-1}) at 300 °C for 1 h. Then, they were cooled down to 50 °C in the same Ar flow. The CO_2 adsorption step was accomplished under a 10% CO_2/He flow (40 cm^3 min^{-1}) at 50 °C for 1 h. Subsequently, the samples were exposed to a flow of Ar (40 cm^3 min^{-1}) for 1 h at 50 °C to remove the reversibly and physically adsorbed CO_2 from the surface. Finally, desorption was carried out from 50 to 600 °C with a heating rate of 10 °C min^{-1} in Ar stream (40 cm^3 min^{-1}).

2.3. Water adsorption properties

In order to evaluate the samples water adsorption properties, these were previously saturated with water vapor under atmospheric conditions (26 ± 2 °C, 0.84 atm). For this purpose, the as-calcined zeolites (0.50 g) were transferred directly from the oven to a closed desiccator containing a saturated aqueous solution of NaCl, which provided a relative humidity of 75 ± 2%. Then, they were stored there for 330 h, monitoring the temperature and humidity by a hygro-thermometer (model 445703, Extech).

After saturation process, the water vapor uptake and the integral water adsorption enthalpy were determined by a non-isothermal method in a simultaneous thermal analyzer TGA-DSC (SDT-Q600, TA instruments). For this, the hydrated zeolites (~0.02 g) were heated from 30 to 500 °C, with a rate of 10 °C min^{-1} under a N_2 flow (100 cm^3 min^{-1}, < 16 ppm H_2O).

Discrimination between the latent heat from the sensible heat involved in the tests, was made by applying two temperature ramps for each prepared adsorbent. The first one, corresponding to the desorption heat, was associated with the phase change of water during the desorption step (ramp 1). Instead, the second one was related to the sensible heat adsorbed by zeolites during heating (ramp 2). After completion of ramp 1, it was assumed that all the adsorbed water was released, and the samples were cooled to 30 °C in the same stream of N_2 (100 cm^3 min^{-1}) to prevent their rehydration. Then, ramp 2 was immediately performed under same conditions as the first one.

Assuming reversibility between the adsorption and desorption processes [22,23], the water vapor uptake was obtained from the first ramp of thermogravimetric analysis and it was normalized by the BET surface area of adsorbents. On the other hand, the integral water adsorption enthalpy, Δh_{ads}, was evaluated using Equation (1) from the thermodynamic model reported by Kim et al. [5]. This equation represents a simple thermodynamic cycle, shown in Scheme 1, comprised by the desorption (a-b), cooling (b-c) and adsorption (c-a) steps. Desorption and cooling steps were monitored by TGA-DSC analysis, while the adsorption process c-a was obtained by applying the First Law of Thermodynamics to the entire cycle a-b-c-a.

$$\Delta h_{ads} = h_{vapor} + \frac{1}{m_{ads(a-b)}}\left(\int_a^b dQ_{ramp1} + \int_a^b h_{vapor}{\cdot}dm_{ads} + \int_b^c dQ_{ramp2}\right) \quad (1)$$

Where, h_{vapor} is the vapor enthalpy at the initial temperature of the thermal analysis, and $m_{ads(a-b)}$ is the water amount released during the desorption (a-b) step between T_a = 30 °C and T_b = 350 °C. dQ_{ramp1} and dQ_{ramp2} correspond to the heat transfer during the desorption (a-b) and cooling (b-c) steps, respectively, which were determinate by the DSC curves.

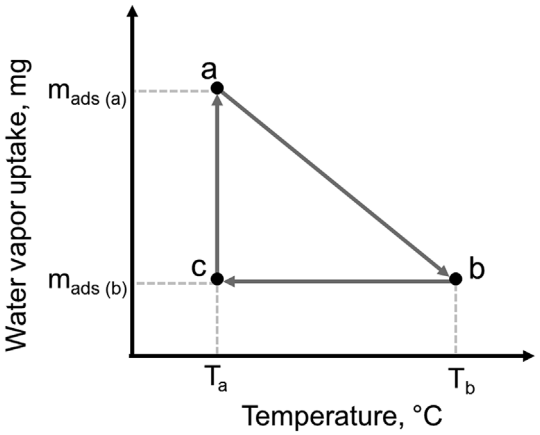

Scheme 1. Theoretical thermodynamic cycle comprising the desorption (process a-b), cooling down (process b-c), adsorption (process c-a) steps to evaluate the water adsorption enthalpy of prepared adsorbents, proposed by Kim et al. [5].

3. Results and discussion

3.1. Characterization of zeolites

The effective metal content of each sample is shown in Table 1. These values indicate that it was possible to modify the parent 5A zeolite with the different amounts of metal, achieving an impregnation efficiency greater than 88%, with respect to the expected nominal value, in all cases.

Table 1 also summarizes the surface area and porosity features of all prepared adsorbents. It was observed that both the surface area and the pore volume of parent zeolite decreased after the impregnation, probably be due to pore blockage by the incorporated metals. Concerning the modified samples, it was appreciated that Ni/5A zeolites suffered greater decrease in BET and micropore surface areas than those containing Ag. This could be related to differences in cation sizes. Ni cations have a lower ionic radius than Ag, and they could occupy in a major extent the narrow pores, leading to a greater pore blockage [23]. Thus, as the accessible pore volume to nitrogen was reduced, not only the total pore volume but also the BET surface area was affected. Because of this partial pore blockage, a similar trend could be appreciated in the surface area of micropores, which was gradually reduced by the increase of the incorporated metal amount.

The crystallographic phases present in the samples and the effect of impregnation on the parent zeolite structure was evaluated by X-ray diffraction. Fig. 1 shows the diffractograms of both the parent and modified materials. It could be seen that all samples exhibited the typical diffraction peaks of the LTA structure (ICDD 01-073-2340, $Na_{12}Al_{12}Si_{12}O_{48}(H_2O)_{27}$), indicating that the crystalline nature of parent zeolite was maintained without any structural change after the incorporation of Ag and Ni. However, in the impregnated samples with the highest amount of metal, an additional crystalline phase was detected. On the one hand, the 20Ag/5A zeolite exhibited three distinctive peaks at 27.1°, 32.6° and 38.3° 2θ degrees, which could be indexed to the (110), (111) and (200) reflections of Ag_2O crystalline phase (ICDD 01-075-1532), respectively. On the other hand, in the case of 20Ni/5A, the peaks at 37.6° (111) and 43.6° (200) 2θ degrees were assigned to the characteristic reflections of NiO crystalline phase (ICDD 01-078-0429). These additional phases were not appreciable in the modified zeolites with 4 and 10 wt% metal. This absence of signal could be related to the low metal amount in the samples or to a high dispersion of metal oxides particles in them [24].

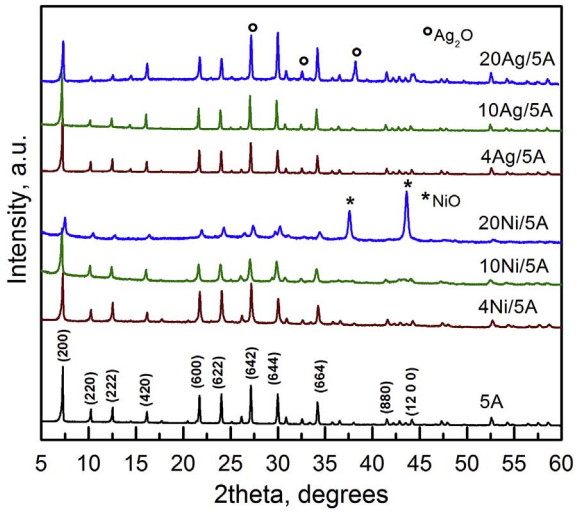

Fig. 1. X-ray diffraction patterns of Ag and Ni modified zeolites.

Comparing with the parent zeolite, it was observed a decrease in the relative intensity of some peaks between 10° and 20° 2θ degrees in samples with 10 and 20 wt% metal. This 2θ region has been correlated to the locations of balancing cations into the zeolite cages [25]. Hence, the change in these characteristic peaks suggests a redistribution of the balancing cations into the zeolite, caused by the metals incorporation.

Infrared spectra of prepared zeolites are presented in Fig. 2. It was observed that the characteristic bands of parent zeolite were preserved in the modified samples spectra. This suggests that the impregnation process did not promote major structural modifications in the zeolite, as

Table 1
Physicochemical properties of parent and modified zeolites.

Sample	Metal content[a], wt%	Surface area, $m^2\ g^{-1}$		Pore volume, $cm^3\ g^{-1}$	
		BET	Micropore[b]	Total pore[c]	Micropore[d]
5A	–	437	410	0.239	0.221
4Ag/5A	3.70	417	384	0.229	0.207
10Ag/5A	9.97	366	336	0.212	0.187
20Ag/5A	20.32	128	115	0.078	0.064
4Ni/5A	3.53	401	342	0.299	0.184
10Ni/5A	9.47	224	169	0.225	0.095
20Ni/5A	19.45	113	82	0.128	0.046

[a] Determined by AAS.
[b] Calculated by the relation $S_{micro} = S_{BET} - S_{ext}$ from the t-plot method.
[c] Total pore volume at $P/P_o = 0.99$.
[d] Calculated by the t-plot method.

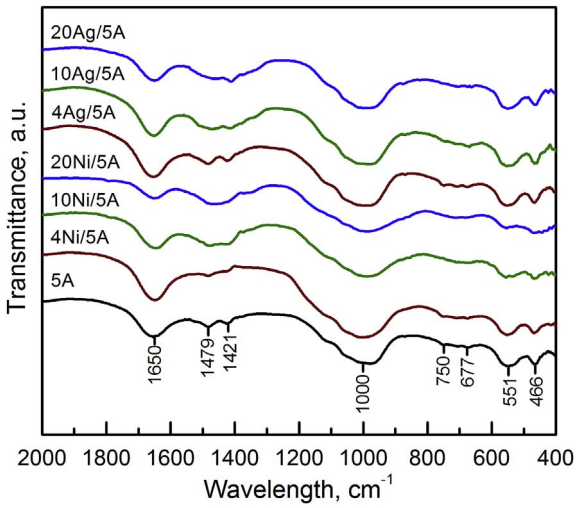

Fig. 2. Mid-infrared spectra of samples.

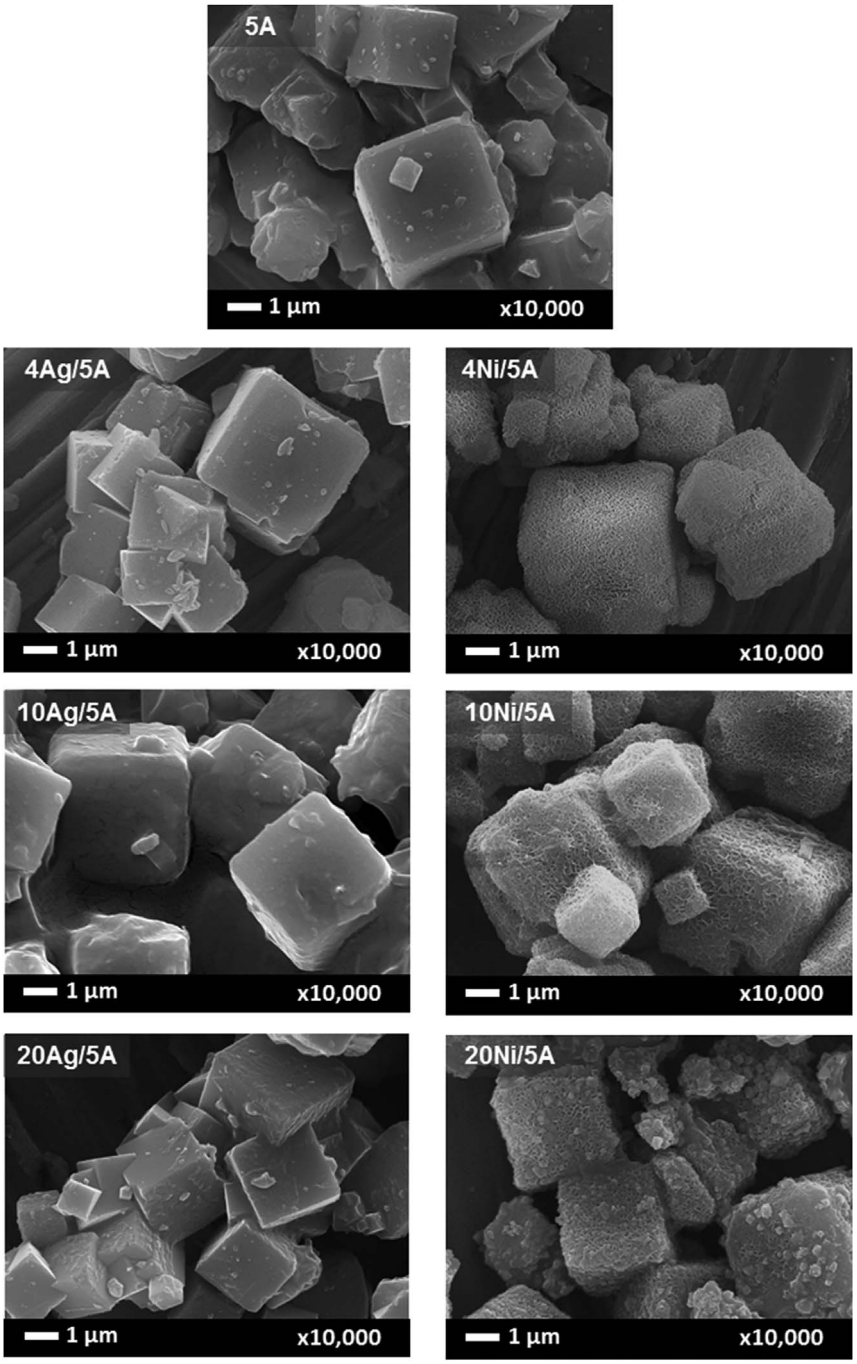

Fig. 3. FE-SEM images of the different modified zeolites.

was observed previously by XRD. For all samples, two high intensity bands were observed at 1000 and 1650 cm^{-1}. The first one was related to the asymmetric stretching of Si-O(Si) and Si-O(Al) bonds, while the second one was assigned to the -OH bending of water molecules and the terminal hydroxyl groups in the zeolite. Other less intense bands at 750, 677 and 466 cm^{-1}, were assigned to the symmetric stretching vibrations of bridge bonds Si-O-Si and Si-O-Al, and to the bending vibrations of O-Si-O bonds respectively. It should be noted that the vibrations occurring at 551 cm^{-1}, due to the symmetrical stretching of the double 4-membered rings in the LTA framework [26], were retained after the impregnation.

Fig. 3 shows the particle morphology of both the parent and the impregnated zeolites. From FE-SEM images, it was observed that the characteristic cubic shape of type A zeolites crystals was retained even after the impregnation. In modified samples, a coating over the crystals was identified, due to the surface deposition of metal species, as was appreciated in the EDS analyses (Fig. S1-S7 in supplementary data). From the EDS mapping, it could be seen that the impregnated metals were well distributed over the zeolites surface. Concerning to the particle size, it could have been expected that the modification with the highest amount of metal led to a greater change. However, from the particle size distributions (PSD) in Fig. S8, it was found that both the 5A zeolite and the modified ones 20Ag/5A and 20Ni/5A, presented a very similar PSD with mean sizes of 2.44 ± 0.61 µm, 2.51 ± 0.57 µm and 2.68 ± 0.54, respectively. Thus, it was observed that neither the shape nor the particle size of 5A zeolite suffered a remarkable change after the impregnation process.

H_2-TPR profiles in Fig. 4 indicate the reductive nature of metal

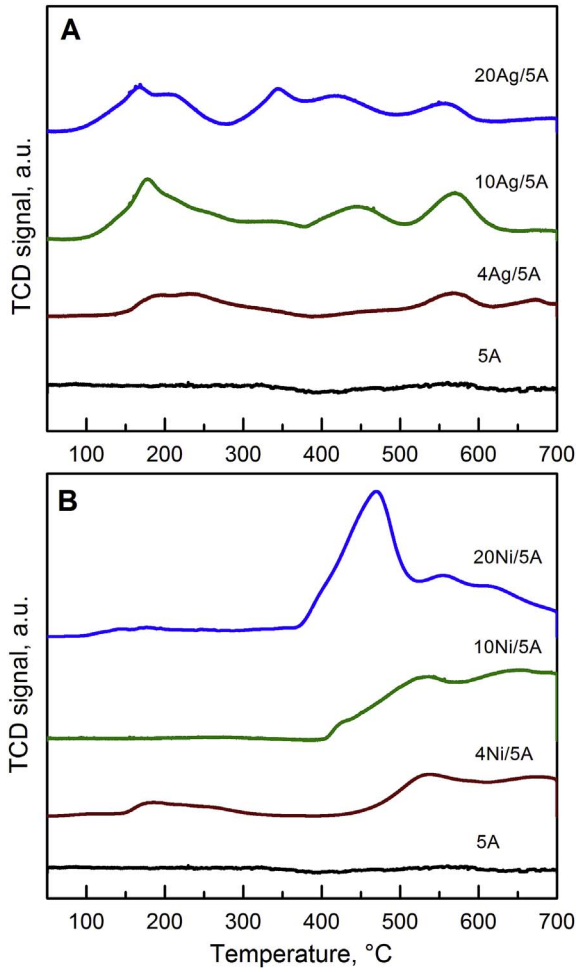

Fig. 4. H_2-TPR profiles of impregnated zeolites, reducibility of Ag/5A (A) and Ni/5A (B) zeolites.

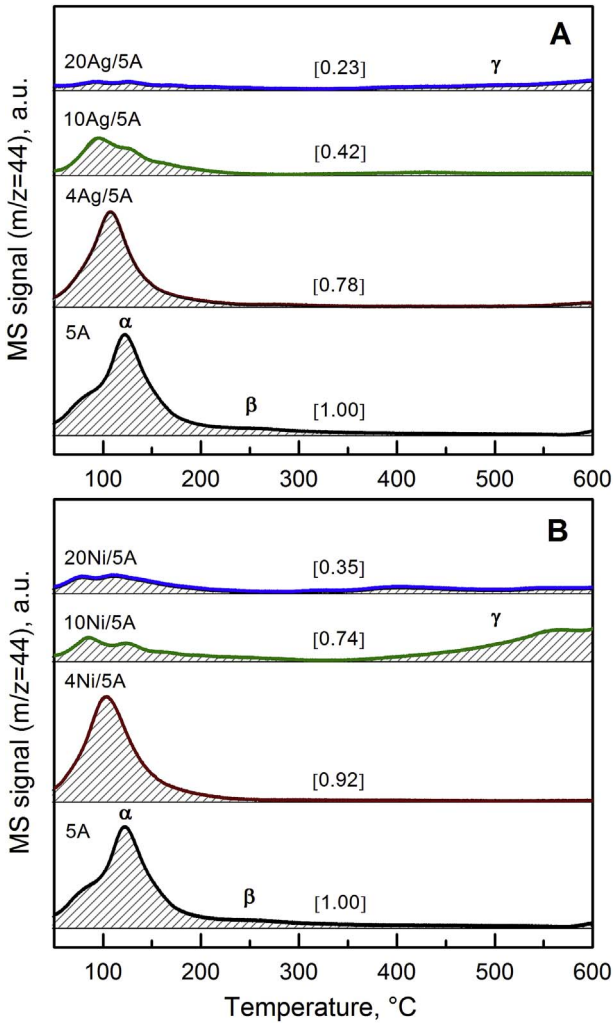

Fig. 5. CO_2-TPD spectra of samples, influence of the nature and amount of Ag (A) and Ni (B) incorporated metal.

species in the prepared adsorbents. For parent zeolite, no reduction signals were observed in the temperature range 50–700 °C, which indicated the absence of reducible species in the sample. Instead, all impregnated zeolites exhibited several reduction signals, which varied in intensity and temperature as function of metal nature and content. Ag/5A samples presented signals with different intensity, from ~100 °C to 700 °C (Fig. 4A). A first group of reduction signals, associated to the reduction of bulk Ag_2O with no or weak interaction with the zeolite, was detected around 150–250 °C [27]. At temperatures between ~300 and ~500 °C, it was observed the reduction of $Ag(I)_xO_y$ clusters inside or on the external surface of the zeolite [28]. Finally, a last group of reduction signals at higher temperatures (~550–600 °C), indicated the reduction of isolated and well dispersed Ag^+ extraframework cations in different sites into the zeolite [29].

In the case of Ni containing samples, the H_2-TPR profiles showed that the reduction began at ~380 °C, and it could not be completed at 700 °C (Fig. 4B). The signal observed at ~470 °C could be assigned to the reduction of bulk NiO [30], while the remaining overlapped signals can be related to the reduction of Ni species of different size, location and interaction with the zeolite [31,32].

It is known that the cations reducibility in zeolites depends on their location into the framework. Cations located in the supercages (α-cages) are more easily reduced at low-temperature than those in the sodalite cages (β-cages) which are reduced at high temperatures [33]. Reduction signals of Ni modified samples centered at high temperatures above ~600 °C, suggests that a great amount of Ni cations could be located in the sodalite cages making them more difficult to reduce.

CO_2-TPD was performed in order to evaluate the effect of incorporated metal on the parent zeolite basicity. Fig. 5 shows the CO_2 desorption profiles of both the unmodified 5A zeolite and those metals impregnated. Three different groups of desorption signals could be identified, low temperature signals around 110 °C (denoted as α), mid-temperature signals between ~200 and ~350 °C (denoted as β), and high-temperature signals above ~350 °C (denoted as γ). The relative amount of desorbed CO_2 was calculated by the integration of each desorption profile (data in brackets). This parameter was defined as the total amount of desorbed CO_2 per gram of sample, in the temperature range of 50–600 °C, with respect to parent zeolite.

5A zeolite exhibited an intense signal between ~50 and ~200 °C, a low shoulder from ~200 to ~350 °C, and no signals at the high temperature range were observed. The first signal, denoted as α, indicated a high presence of weak basic sites, while the low β shoulder suggested a smaller amount of sites with medium basic strength. Concerning the metal modified samples, an additional low intensity signal, denoted as γ, was observed above ~350 °C in the zeolite 10Ni/5A and, more tenuously, in the 20Ni/5A and 20Ag/5A zeolites. This evidenced the formation of strongly adsorbed CO_2 and hence the presence of strong basic sites in these samples.

The multiple desorption signals observed in the CO_2-TPD profiles, revealed the heterogeneity of their basic sites strength. This effect could be associated to changes in the charge distribution of the oxygen atoms in framework, their angles and bond length, and their interactions with

the incorporated metals [34,35].

It could be seen that the metals incorporation led to a decrease in the weak basic sites, as well as in the total basicity of 5A zeolite (data in brackets). This decrease could be due to different effects. On the one hand, as was indicated in the porosity analyses, the formed oxides could block some pores during the impregnation, preventing the access of CO_2 to the basic centers in them. On the other hand, the extraframework cations, corresponding to Lewis acids, could have interacted with some oxygen atoms of the framework, making them unavailable to react with the CO_2 or allowing just weak reactions [34,36].

Although Ag-modified zeolites were expected to exhibit higher adsorption of CO_2 due to their higher porosity and surface area, it was observed that these samples had a greater decrease in the total basicity than those containing Ni. This could be related to the fact that Ni cations could interact with more CO_2 molecules than Ag ones, due to their strong polarizing power (Z^+/r^2_{ionic} = 4.2 and 0.8 for Ni^{2+} and Ag^+, respectively) [37].

Considering all the physico-chemical characterizations carried out, it can be established that the impregnation process used was suitable for adding metals on the zeolite surface, as well as to have a cation exchange in some extent. Similar behavior was also observed in previous works with other metal modified zeolites prepared by different chemical methods [19,38,39].

3.2. Water adsorption properties

TGA curves in Fig. 6A1 and 6A2 show the weight loss of Ag/5A and Ni/5A samples, respectively, as well as of the parent zeolite. The observed weight loss was associated with the water desorption by heating. Water desorption profile started at 30 °C and was completed around 400 °C. Comparing the TGA ramps 1 and 2, it was observed that in ramp 2 the amount of desorbed water was almost negligible. This confirms that in this ramp, zeolites were in a dry state or, at least, almost all the adsorbed water was released during the first heating ramp.

Fig. 6B1 and 6B2 shows the respective differential thermogravimetric (DTG) curves of Ag/5A and Ni/5A samples. For all adsorbents, two main temperature regions of weight loss could be identified. The first one, from 30 to ~120 °C, and the second one between ~120 and ~400 °C. In zeolites, water adsorption occurs initially in the most active sites, i.e. the framework oxygens and the balancing cations, which involves high energies [40]. As water vapor uptake increase, these main adsorption sites in zeolites are occupied, and the adsorption takes place on the less active sites, involving lower energies [41]. According to these interactions, during heating the weakly adsorbed molecules will be released first, and later the strongest ones bound to the zeolite framework. Thus, the first weight loss, could be attributed to the release of physically adsorbed water. In contrast, the second weight loss, could be associated with the release of water molecules strongly adsorbed and chemically bound to the non-framework cations and framework oxygens of zeolite [23,40].

Regarding to the modified samples, it was observed that weight loss, caused by the water desorption, was lower for Ni-modified zeolites than those with Ag. As was suggested by the H_2-TPR profiles, Ni cations could have been more easily located in β-cages than Ag cations, which are preferred to be located in α-cages [40]. A higher amount of Ni cations located in the most hydrophilic sites (β-cages), could have produced a steric effect and limit the access of water molecules, decreasing the total amount of water adsorbed in them. In addition, it was appreciated that the metals impregnation led to a shift in the DTG profiles towards lower desorption temperatures, which could suggest a decrease in hydrophilic character of zeolites. This effect could increase the zeolites use in thermal applications with low desorption temperatures requirements [42,43].

Differential Scanning Calorimetry (DSC) profiles of both the

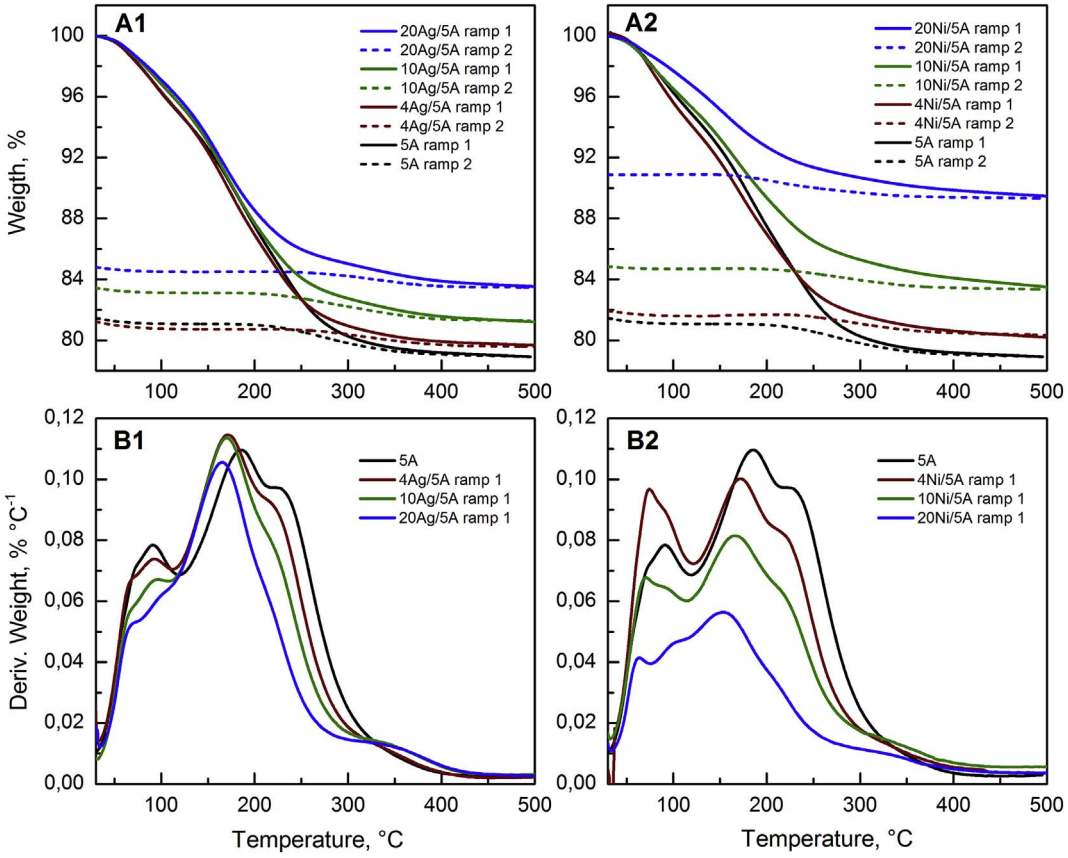

Fig. 6. TGA analysis of Ag/5A (A1) and Ni/5A (A2) zeolites and their respective DTG curves Ag/5A (B1) and Ni/5A (B2).

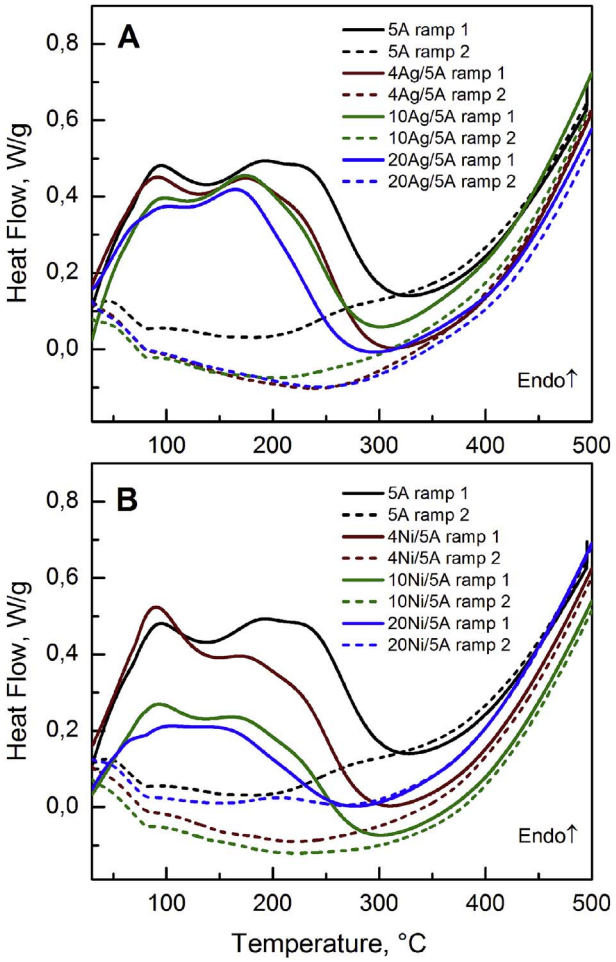

Fig. 7. DSC profiles of Ag/5A (A) and Ni/5A (B) prepared adsorbents.

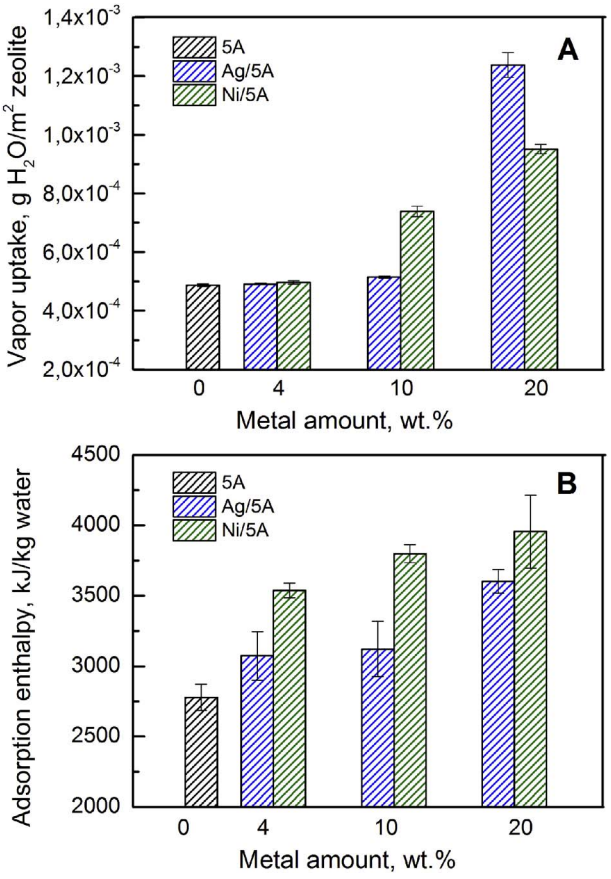

Fig. 8. Water adsorption properties of prepared adsorbents: water vapor uptake (A) and water adsorption enthalpy (B).

hydrated and dried adsorbents are shown in Fig. 7. For all samples, it is clearly seen that ramp 1 exhibited a higher heat flow compared to ramp 2. This was because the latent heat transferred during the water desorption in first ramps, implied a greater heat flow than only the sensible heat of dry adsorbents involved in the second ramps. Otherwise, the DSC thermograms revealed the endothermic character of the weight losses observed in the DTG curves. As was mentioned previously, these thermal events could be ascribed to the desorption of water molecules located in diverse adsorption sites, with different interaction energies. Thus, the first thermal event from 30 to ~130 °C indicated a lower energy requirement to release the weakly bound water. Instead, the second event, from ~130 to ~320 °C, was related to a greater amount of energy to desorb the more strongly attached water. The increase in heat flow from ~320 °C, was attributed to the sensible heat required by samples to raise their temperature, confirmed by the similar behavior of all samples in this region.

On the other hand, it was observed that the metals incorporation led to a decrease in the water desorption heat. Fig. 7A and B shows the DSC curves of Ag/5A and Ni/5A samples, respectively. Regarding to the incorporated metal, it was seen that Ni-modified zeolites exhibited a lower desorption heat than those containing Ag. As a result of their greater charge, Ni cations were expected to require more energy to desorb the water molecules. However, these samples presented a greater pore blockage, which could have promoted the water adsorption in more superficial sites, and thus, were more easily released during heating.

Water adsorption results of prepared adsorbents are shown in Fig. 8. It was observed that Ag and Ni metals had a considerable influence on water adsorption properties of the parent zeolite. Fig. 8A shows the water vapor uptake, normalized by the BET surface area of adsorbents, as a function of the incorporated metal. It was found that, after the impregnation, the water vapor uptake of samples was increased with the metal amount. This suggests that the incorporation of metal species favored the superficial adsorption of water molecules per available area of zeolite. Comparing the incorporated metal nature, no substantial difference between 4Ag/5A and 4Ni/5A samples was perceived. For the zeolites modified with 10 wt% of metal, it was observed that the Ni-modified ones exhibited a greater water vapor uptake than those containing Ag. Instead, when the metal amount increased to 20 wt%, the opposite trend was obtained. These differences in the water vapor uptake may be related to the distribution of metal species, water diffusivity as well as the different water-metal, water-zeolite and metal-zeolite interactions in the impregnated samples [23]. In this work, an experimental approach was done to understand the effect of metals on the maximum water vapor uptake in zeolites, however, further studies must be conducted to find the most relevant factors that determine the maximum water adsorption of these materials.

On the other hand, Fig. 8B shows the water adsorption enthalpy of samples. It was clearly seen that the metals impregnation led to an increase in the water adsorption enthalpy of the parent zeolite, with the increase in the metal content. Regarding the incorporated metal, Ni/5A zeolites exhibited a higher water enthalpy adsorption than Ag/5A samples. This could be related to the differences in the cations hydration enthalpies and their ionic charge. It is known that the hydration enthalpy of Ni cations is much larger than Ag cations and, therefore, this could contribute with a greater energy in the hydration process during the water adsorption [44,45]. In addition, the attraction energy of polar water molecules is greater when they interact with high charge density cations as Ni. Thus, from the observed results, Ni atoms in close contact with zeolites seems to favored the interaction of water

molecules with the support. Nevertheless, from XRD and FE-SEM results, it was observed that some agglomerates of NiO where formed in zeolites with high Ni content. In that sense, nickel oxide particles that are not in close contact with zeolites atoms could no contribute in a high extent to the adsorption process. On the other hand, adsorbent with high Ag content showed high dispersion of metal and less amount of metal oxide particles, as could be observed by FE-SEM [12]. Consequently, the hydration enthalpy of Ni-modified samples will be higher than those containing Ag.

This tailoring in the water adsorption properties of zeolites, modified by metals impregnation, could offer an attractive potential to tune their adsorption behavior in thermal storage applications and waste heat recovery systems.

4. Conclusions

In this work, 5A zeolite was successfully modified by wet impregnation with different amounts (4, 10 and 20 wt%) of Ag and Ni metals. Characterization results showed that metals were well distributed in different sites into the 5A zeolite preserving its crystal structure and morphological characteristics in all the prepared materials. Ag and Ni metals had a remarkable influence on the physicochemical properties of parent zeolite, indeed, a decrease in the weak basic sites, as well as in its total basicity was observed.

Although, the surface area of parent zeolite was decreased after the impregnation, thermal analyses showed that the metal incorporation caused an increase in the adsorption enthalpy values, which is favorable for thermal applications. Additionally, it was observed a shift in the DTG profiles towards lower desorption temperatures, which could suggest a decrease in hydrophilic character of zeolites. This effect could be attractive to use these materials in thermal applications with low desorption temperatures requirements, such as, thermal energy storage and waste heat recovery systems. However, it is worth to notice, that the performance of these adsorbents strongly depends on the thermodynamic cycle in which they would be proved.

Acknowledgements

The authors wish to thank to the Instituto Tecnológico Metropolitano (Project P14209 and “Programa Piloto de Pasantías 2016”) for the financial support. The author M.R-S acknowledge also the support of FONDECYT (CONICYT) through the Postdoctoral Project 3140536.

Appendix A. Supplementary data

Supplementary data related to this article can be found at http://dx.doi.org/10.1016/j.micromeso.2018.02.036.

References

[1] K.E. N'Tsoukpoe, H. Liu, N. Le Pierrès, L. Luo, Renew. Sustain. Energy Rev. 13 (2009) 2385–2396.
[2] H. Demir, M. Mobedi, S. Ülkü, Renew. Sustain. Energy Rev. 12 (2008) 2381–2403.
[3] S.K. Henninger, S.J. Ernst, L. Gordeeva, P. Bendix, D. Fröhlich, A.D. Grekova, L. Bonaccorsi, Y. Aristov, J. Jaenchen, Renew. Energy 110 (2017) 59–68.
[4] Y.I. Aristov, Appl. Therm. Eng. 50 (2013) 1610–1618.
[5] H. Kim, H.J. Cho, S. Narayanan, S. Yang, H. Furukawa, S. Schiffres, X. Li, Y.-B. Zhang, J. Jiang, O.M. Yaghi, E.N. Wang, Sci. Rep. 6 (2016) 19097.
[6] S.K. Henninger, F. Jeremias, H. Kummer, P. Schossig, H.M. Henning, Energy Procedia 30 (2012) 279–288.
[7] P. Tatsidjodoung, N. Le Pierrès, L. Luo, Renew. Sustain. Energy Rev. 18 (2013) 327–349.
[8] L.W. Wang, R.Z. Wang, R.G. Oliveira, Renew. Sustain. Energy Rev. 13 (2009) 518–534.
[9] L. Bonaccorsi, L. Calabrese, S. Alioto, P. Bruzzaniti, E. Proverbio, Renew. Energy 110 (2017) 79–86.
[10] S.K. Henninger, F.P. Schmidt, H.M. Henning, Appl. Therm. Eng. 30 (2010) 1692–1702.
[11] J. Jänchen, D. Ackermann, H. Stach, W. Brösicke, Sol. Energy 76 (2004) 339–344.
[12] U.D. Joshi, P.N. Joshi, S.S. Tamhankar, V.P. Joshi, B.B. Idage, V.V. Joshi, V.P. Shiralkar, Thermochim. Acta 387 (2002) 121–130.
[13] T.H. Herzog, J. Jänchen, E.M. Kontogeorgopoulos, W. Lutz, Energy Procedia 48 (2014) 380–383.
[14] J. Jänchen, H. Stach, U. Hellwig, Water Sorption in Faujasite- and Chabazite Type Zeolites of Varying Lattice Composition for Heat Storage Applications, Elsevier B.V., 2008.
[15] L. Scapino, H.A. Zondag, J. Van Bael, J. Diriken, C.C.M. Rindt, Appl. Energy 190 (2017) 920–948.
[16] L.Y. Dolgikh, I.L. Stolyarchuk, P.E. Strizhak, A.V. Shvets, V.G. Il'in, Theor. Exp. Chem. 42 (2006) 33–38.
[17] L.P. Ozorio, R. Pianzolli, L. Da Cruz MacHado, J.L. Miranda, C.C. Turci, A.C.O. Guerra, E.F. Souza-Aguiar, C.J.A. Mota, Appl. Catal. Gen. 504 (2015) 187–191.
[18] D. Zhang, H. Zhang, Y. Yan, Microporous Mesoporous Mater. 243 (2017) 193–200.
[19] M. Romero-Sáez, D. Divakar, A. Aranzabal, J.R. González-Velasco, J.A. González-Marcos, Appl. Catal. B Environ. 180 (2016) 210–218.
[20] S. Brunauer, P.H. Emmett, E. Teller, J. Am. Chem. Soc. 60 (1938) 309–319.
[21] B.C. Lippens, J.H. de Boer, J. Catal. 4 (1965) 319–323.
[22] M. Afzal, G. Yasmeen, M. Saleem, P. Butt, A. Khattak, J. Afzal, J. Therm. Anal. Calorim. 62 (2000) 721–727.
[23] F. Benaliouche, N. Hidous, M. Guerza, Y. Zouad, Y. Boucheffa, Microporous Mesoporous Mater. 209 (2015) 184–188.
[24] K. Van Der Borght, V.V. Galvita, G.B. Marin, Appl. Catal. Gen. 492 (2015) 117–126.
[25] A.M. Fonseca, I.C. Neves, Microporous Mesoporous Mater. 181 (2013) 83–87.
[26] W. Mozgawa, M. Król, K. Barczyk, Chemik 65 (2011) 671–674.
[27] S.W. Baek, J.R. Kim, S.K. Ihm, Catal. Today 93–95 (2004) 575–581.
[28] A. Musi, P. Massiani, D. Brouri, J.M. Trichard, P. Da Costa, Catal. Lett. 128 (2009) 25–30.
[29] K.A. Bethke, H.H. Kung, J. Catal. 172 (1997) 93–102.
[30] Y. Wu, A. Yan, Y. He, B. Wu, T. Wu, Catal. Today 158 (2010) 258–262.
[31] A.J. Maia, B. Louis, Y.L. Lam, M.M. Pereira, J. Catal. 269 (2010) 103–109.
[32] Y. Shen, A.C. Lua, RSC Adv. 4 (2014) 42159–42167.
[33] M. Afzal, G. Yasmeen, M. Saleem, J. Afzal, J. Therm. Anal. Calorim. 62 (2000) 277–284.
[34] J.A. Lercher, A. Jentys, A. Brait, Mol. Sieves - Sci. Technol. 6 (2008) 153–212.
[35] D. Barthomeuf, Microporous Mesoporous Mater. 66 (2003) 1–14.
[36] P.J. Smeets, J.S. Woertink, B.F. Sels, E.I. Solomon, R.A. Schoonheydt, Inorg. Chem. 49 (2010) 3573–3583.
[37] D. Bonenfant, M. Kharoune, P. Niquette, M. Mimeault, R. Hausler, Sci. Technol. Adv. Mater. 9 (2008) 13007.
[38] O. Kikhtyanin, R. Bulánek, K. Frolich, J. Čejka, D. Kubička, J. Mol. Catal. Chem. 424 (2016) 358–368.
[39] H.Y. Zheng, J.Z. Wang, Z. Li, L.F. Yan, J.Z. Wen, Fuel Process. Technol. 152 (2016) 367–374.
[40] P. Castaldi, L. Santona, C. Cozza, V. Giuliano, C. Abbruzzese, V. Nastro, P. Melis, J. Mol. Struct. 734 (2005) 99–105.
[41] D. Mihoubi, A. Bellagi, J. Chem. Thermodyn. 38 (2006) 1105–1110.
[42] T. Kohler, K. Müller, Energy Sci. Eng 5 (2017) 21–29.
[43] W.K. Mekhamer, Arab. J. Chem. 9 (2016) S264–S268.
[44] H. Sun, D. Wu, K. Liu, X. Guo, A. Navrotsky, J. Phys. Chem. C 120 (2016) 15251–15256.
[45] N. Petrova, T. Mizota, K. Fujiwara, J. Therm. Anal. Calorim. 64 (2001) 157–166.